Journal of Research and Applications in Mechanical Engineering
ISSN: 2229-2152 (Print); 2697-424x (Online)
(2025) Vol. 13, No. 3, Paper No. JRAME 25-13-045
[DOI: 10.14456/ jrame.2025.45]

Research Article

A Shape Optimization Approach to the Design of a Cartilage Plate Used in Cartilage Tympanoplasty

Z. Wu[1,*]
K. Okamoto[2]
T. Shigeyoshi[2]
[1] *Department of Mechanical Systems Engineering, The University of Shiga Prefecture, Shiga, 522-8533, Japan*
[2] *Graduate School of Engineering, The University of Shiga Prefecture, Shiga, 522-8533, Japan*

Received 20 October 2024
Revised 4 January 2025
Accepted 6 January 2025

Abstract:
This paper presents a shape optimization approach for a cartilage plate used in cartilage tympanoplasty to more closely approximate the original auditory characteristics of the human ear. First, we constructed a finite element model based on the geometric data of the middle ear, including the tympanic membrane, ossicles, and surrounding muscles. We then proposed a shape optimization method for designing the cartilage plate. The optimization problem was formulated with an objective function defined as the least squares difference between the amplitudes of the stapes post-repair and those in the healthy state across a wide frequency range. To enhance computational efficiency, we derived the shape gradient function and developed a method to calculate it using modal parameters. We employed the H^1 gradient method for shape modification. Finally, two numerical examples, using a combination of CAE software and a custom program, were conducted. In an idealized model, the objective function decreased by 98%, while in a repaired tympanic membrane model, it decreased by 43%, demonstrating the effectiveness of our approach.

Keywords: *Shape optimization, Myringoplasty, Cartilage tympanoplasty, Tympanic membrane perforation, FEM analysis*

1. Introduction

Tympanic membrane (TM) perforation is a common condition that may require surgical treatment, especially when it recurs. One widely used procedure is cartilage tympanoplasty, which involves harvesting cartilage from the patient's auricle and using it to repair the damaged area of the TM. Typically, the cartilage is sliced into thin plates with a thickness ranging from 0.1 mm to 0.7 mm. However, in cases of large perforations, the auditory function after repair often does not fully recover to its pre-injury state. This limitation arises from the significant differences in material properties between cartilage and the native tympanic membrane.

The ability of the middle ear to transmit sound depends on its vibration behavior. To improve hearing through surgery, it is important to make the repaired TM vibrate as closely as possible to a healthy one. In mechanical engineering, techniques like shape optimization are commonly used to control vibrations and improve the performance of mechanical structures. Inspired by these ideas, this study attempts to apply shape optimization methods from mechanical engineering to solve problems in TM reconstruction.

To improve patients' quality of life (QOL), extensive efforts have been made to develop improved surgical techniques. To mitigate the risks associated with human ear experiments, many studies have utilized numerical analysis as an alternative approach to refine surgical methods. Since the early 1990s, the Finite Element Method (FEM) has been employed to model the complex dynamics of the middle ear. FEM allows for the simulation of the mechanical

* Corresponding author: Z. Wu
E-mail address: wu.z@mech.usp.ac.jp

behavior of the middle ear under various conditions without physical intervention. Pioneering work by Wada et al. [1] introduced a basic finite element model of the middle ear, which was later expanded to include muscles, ligaments, and ossicular joints [2]. These early models provided a foundation for further research that refined the representation of middle ear anatomy and its dynamic responses [3], [4]. Further research has focused on understanding the middle ear's dynamic behavior when the TM is perforated [5], [6].

However, accurately modeling the middle ear remains challenging due to difficulties in capturing soft tissues like ligaments, muscles, and ossicular joints using conventional imaging techniques such as micro-CT. These soft tissues play essential roles in the mechanical function of the middle ear, influencing sound transmission and overall system response. Simplifications in numerical models often reduce accuracy. To address this, De Greef et al. [7] employed phosphotungstic acid staining to enhance soft tissue contrast, enabling more precise imaging of the middle ear's anatomical structures, including ligaments and joints, and facilitating more accurate finite element modeling of its biomechanics.

There are also several studies concerning the improvement of cartilage tympanoplasty. Zahnert et al. [8] measured the Young's modulus of conchal and tragal cartilage and evaluated the effect of cartilage thickness on acoustic transfer experimentally, confirming that a thickness of 500 μm or less reduces acoustic transfer loss. These findings provide valuable insights into the use of cartilage for TM reconstruction. Lee et al. [9] used finite element analysis to determine the optimal thickness of cartilage grafts for TM perforation repair. The results suggest that, for medium and large perforations, thinner grafts enhance sound transmission.

In previous studies on the optimal thickness of cartilage, the cartilage plate was assumed to have a uniform thickness. Here, we consider an alternative approach to cartilage tympanoplasty by varying the thickness of the cartilage plate and optimizing its distribution to better approximate the original auditory characteristics of the human ear. Our objective is to optimize the design of the cartilage plate used for TM repair so that the vibration characteristics of the repaired membrane resemble those of a healthy TM. Specifically, within a certain frequency range, we aim to bring the amplitude of the stapes vibrations closer to that of the healthy ear. To address this optimization problem, the shape optimization approach should treat the problem of amplitude regulation over a broad frequency range. Shape optimization techniques have been widely used to enhance structural strength [10] or reduce vibration levels [11]. However, to the best of our knowledge, these methods have not yet been applied to amplitude regulation over a broad frequency range.

As stated above, this study is motivated by the need to enhance the auditory performance of repaired tympanic membranes, addressing limitations in existing surgical methods. For this purpose, we proposed a shape optimization approach for the problem of amplitude regulation over a broad frequency range. We first construct a finite element model of the middle ear, and confirm the validity of numerical model. We then define the objective function for amplitude regulation over a broad frequency range, and formulate the optimization problem. Subsequently, we derive the shape gradient function, and develop a shape optimization system. Finally, we provide numerical examples to illustrate the effectiveness of our method. By leveraging shape optimization techniques, this approach not only advances the field of tympanic membrane reconstruction but also illustrates the potential for methodologies to achieve a desired vibration characteristic over a broad frequency range in the mechanical engineering field.

2. Middle-Ear System and its Numerical Model

A numerical model of the middle ear system was constructed using geometric data downloaded from the University of Antwerp website [12]. As shown in Fig. 1, it is a finite element (FE) model that includes the TM, ossicles, ligaments, joints, the stapedius muscle, and other structures. The names of all components, labeled from a to o in Fig. 1, along with their material properties, are listed in Table 1 [4], [13], [14]. Figure 2 shows the boundary condition in which the nodes at the circumference of the tympanic annular ring, along with the attachment points of the tensor tympani tendon, each ligament, and the stapedius muscle, were constrained. The cochlea contains a watery fluid that oscillates in response to vibrations from the middle ear. Additionally, its complex structure makes it difficult to model. Therefore, to simplify this, the cochlear fluid's viscosity was represented by a damper. The damper was attached to the bottom of the stapes footplate, and its damping coefficient was specified as 0.06 Ns/m [3]. A pressure of 0.632 Pa, calculated from a sound pressure level of 90 dB, was applied to the surface of the TM as the load condition. The amplitude and frequency at the stapes footplate (SFP) are closely related to the strength of stimulation to the inner ear. Therefore, an analysis of the stapes base amplitude was conducted by applying a sound pressure level of 90 dB

to the TM over a frequency range of 0.25 kHz to 8 kHz. The frequency response of the amplitude is shown as a red line in Fig. 3. The analysis results were then compared with a measurement curve [15]. It was observed that the analyzed curve mostly lies between the lower and upper bounds of the measured curve, except for a small frequency range. Notably, there is a peak response around 1.0 kHz, which is close to the peak position of the measured curve.

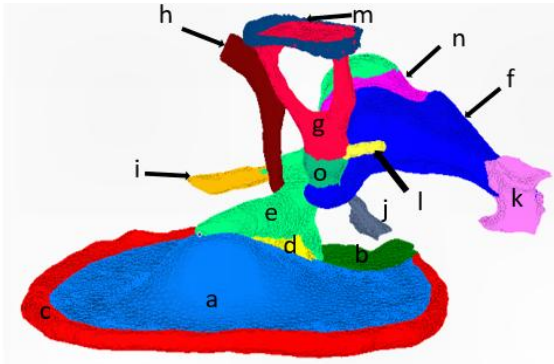

Fig. 1. FE model of the middle ear system.

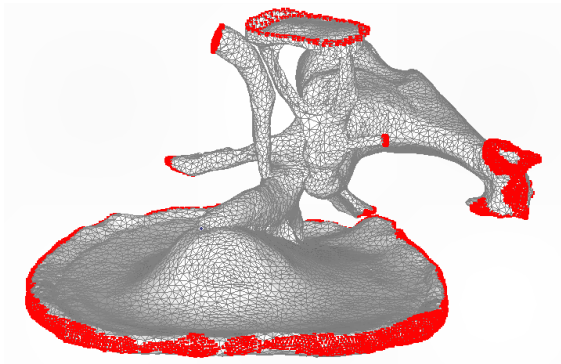

Fig. 2. Constraint points in FE model.

Table 1: Material properties of the parts of the middle ear.

		Young's Modulus[MPa]	Density[kg/m^3]
a	Pars tensa of TM	33.4	1200
b	Pars flaccida of TM	11.1	1200
c	Tympanic annular ring	0.6	1200
d	Manubrium fold	3.34	1200
e	Malleus	14000	2390
f	Incus	14100	2150
g	Stapes	14000	2200
h	Tensor tympani tendon	5	1200
i	Anterior mallear ligament	21	1200
j	Lateral mallear ligament	6.7	1200
k	Posterior incudal ligament	4.8	1200
l	Stapedius muscle tendon	0.38	1200
m	Stapes annular ligament	0.15	1200
n	Incudomallear joint	7	1200
o	Incudostapedial joint	6	1200

As shown in Fig. 4, simulations were also conducted for the perforated TM and the repaired TM with a cartilage plate. In the repaired models, the thicknesses of cartilage plate were set to 0.3mm, 0.5mm, and 0.7mm, respectively. The Young's Modulus of the cartilage is set to 2.8MPa [8], which is quite different from that of the TM, and the density was set to 1300 kg/m^3

The frequency response curve of stapes footplate of each model was shown in Fig. 5. It can be found that the displacement of the stapes footplate with TM perforation is significantly reduced across all frequency ranges compared to that of a healthy middle ear. This reduction is considered to be due to the decreased load-bearing surface caused by the perforation. When the TM was repaired with cartilage, the displacement of the stapes footplate in the 0.25 kHz to 2.0 kHz range was observed to approach that of a healthy ear compared to the perforated condition. However, there are still large differences remained in all models, especially beyond the 1.0 kHz frequency range. Additionally, the peak frequency of all cartilage TM models was observed to decrease compared to the healthy condition, likely due to cartilage having a lower Young's modulus than the natural TM.

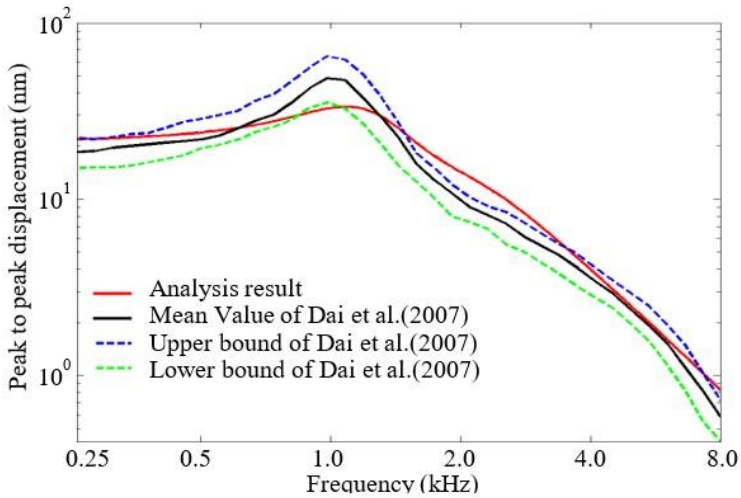

Fig. 3. Comparison of analysis result of our mode and measured data of other studies.

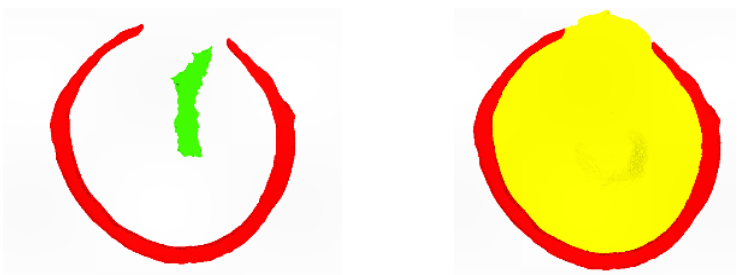

(a) Perforated TM (b) Repaired TM with cartilage

Fig. 4. FE model of perforated TM and repaired TM.

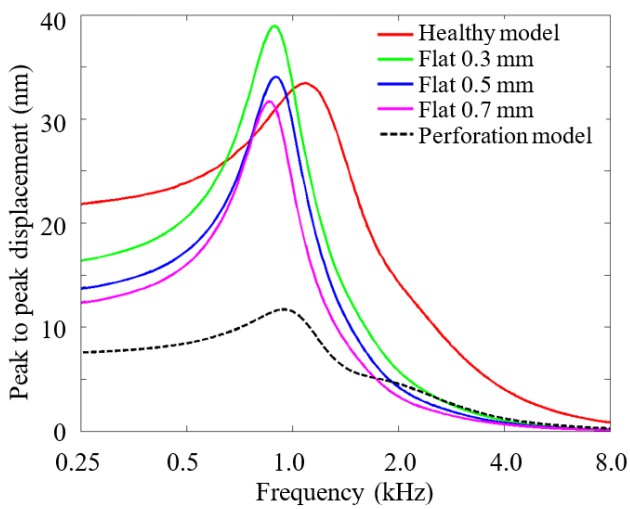

Fig. 5. Comparison of SFP amplitude of healthy, perforation and uniform cartilage plates.

These results suggest that cartilage repair of TM perforation can lead to some improvement in stapes footplate displacement. However, simply adjusting the thickness of the TM does not address the reduction in peak frequency, and the repaired membrane does not fully replicate the characteristics of a healthy TM. To increase the peak

frequency, enhancing the stiffness of the cartilage TM is considered necessary. Therefore, optimizing the thickness distribution of the cartilage membrane may increase its stiffness, allowing it to achieve characteristics that more closely match those of a healthy TM.

3. Shape Optimization Method for Auditory Amplitude Matching

We consider the shape optimization problem of a cartilage plate to improve auditory characteristics by matching the SFP displacement after repair to that observed in a healthy ear across a wide frequency range. Initially, we focus on an optimization problem aimed at matching the SFP displacement at a single frequency. This approach is then extended to an optimization problem over a wide frequency range.

3.1 Governing equation of the frequency response problem

As a preparation for the formation of a shape optimization problem, the governing equation of the frequency response problem with viscous dampers is stated.

An elastic continuum, which occupies a domain $\Omega \subset \mathbb{R}^d, d = 2,3$, and has a boundary Γ is considered. The continuum is fixed on the boundary $\Gamma_1 \subset \Gamma$, supported by viscous dampers at local points, and excited by an excitation force $\boldsymbol{p}(t)$ on the boundary $\Gamma_2 = \Gamma \setminus \Gamma_1$. When $\boldsymbol{p}(t)$ is a harmonic force with angular frequency ω, both $\boldsymbol{p}(t)$ and its response $\tilde{\boldsymbol{u}}(t)$ can be represented as:

$$\boldsymbol{p}(t) = \boldsymbol{P}e^{j\omega t}, \quad \tilde{\boldsymbol{u}}(t) = \boldsymbol{u}e^{j\omega t} \tag{1}$$

where P is the amplitude of the force, and $\boldsymbol{u}$ is the complex amplitude of $\tilde{\boldsymbol{u}}(t)$. For the sake of convenience in the derivation of the sensitivity function, we use the variational form of the equation of motion as the governing equation:

$$a(\boldsymbol{u}, \boldsymbol{v}) + j\omega c(\boldsymbol{u}, \boldsymbol{v}) - \omega^2 b(\boldsymbol{u}, \boldsymbol{v}) = l(\boldsymbol{P}, \boldsymbol{v}), \ \ \forall \boldsymbol{v} \text{ in } \Omega \tag{2}$$

where $\boldsymbol{v}$ is the variation of $\boldsymbol{u}$. Bilinear forms of $a(\cdot\,,\,\cdot)$, $b(\cdot\,,\,\cdot)$, $c(\cdot\,,\,\cdot)$ and $l(\cdot\,,\,\cdot)$ are defined as Eqs. (3)-(6). In this study, to account for the effects of Rayleigh damping and viscous dampers, the damping force term is represented as shown in Eq. (5). Here, α and β denote the Rayleigh damping coefficients. For simplicity, we assume an ideal viscous damper, where the damper's stiffness and mass are considered negligible. The parameter c_{dm} is the damping coefficient for the *dm*-degree of freedom, and x_{dm} represents its position.

$$a(\boldsymbol{u}, \boldsymbol{v}) = \int_\Omega C_{ijkl} u_{k,l} v_{i,j} dx \tag{3}$$

$$b(\boldsymbol{u}, \boldsymbol{v}) = \int_\Omega \rho u_i v_i dx \tag{4}$$

$$c(\boldsymbol{u}, \boldsymbol{v}) = \beta a(\boldsymbol{u}, \boldsymbol{v}) + \alpha b(\boldsymbol{u}, \boldsymbol{v}) + \sum_{m=1}^{N} \int_\Omega c_{dm} \delta(x - x_{dm}) u_i v_i dx \tag{5}$$

$$l(\boldsymbol{P}, \boldsymbol{v}) = \int_{\Gamma_2} P_i v_i d\Gamma \tag{6}$$

where C_{ijkl} represents the elastic stiffness tensor, N is the number of dampers, and $\delta(\cdot)$ denotes the Dirac's delta function. The Einstein summation convention and partial differential notation $(\cdot)_{,i} \equiv \partial(\cdot)/\partial x_i$ are used for convenience.

3.2 Objective function and formulation under frequency excitation

Consider the problem of shape optimization, where the goal is to determine the magnitude of the complex amplitude $u_{x0}(\omega)$ at position $\boldsymbol{x}_0$ under single-frequency excitation so that it meets a specified value $\bar{u}_{x0}(\omega)$. For this amplitude regulation problem, the objective function can be set as follows:

$$F(\omega) = |f\ (\omega)| = \left|u_{x0}(\omega) \cdot {u_{x0}}^*(\omega) - {\bar{u}_{x0}}^2(\omega)\right| = \left|\int_\Omega \delta(\boldsymbol{x} - \boldsymbol{x}_0) \boldsymbol{u} \cdot \boldsymbol{u}^*\, d\Omega - {\bar{u}_{x0}}^2(\omega)\right| \tag{7}$$

where $(\cdot)^*$ represents a conjugate complex number of $(\cdot)$. Then we introduce a mass constraint to the shape optimization problem as

$$m = \int_{\Omega_s} \rho dx \leq M \tag{8}$$

where m denotes the mass, M represents the upper mass limit, and ρ is the density.
We use a non-parametric approach to the shape optimization. Expressing the domain variation with a velocity field $\boldsymbol{V}(x), x \in \Omega$ [16], then this shape optimization problem can be formulated as:

find	$\boldsymbol{V}(x)$
that minimize	$F(\omega)$
subject to	Eq. (2), Eq. (8) and
	$a(\boldsymbol{u}^*, \boldsymbol{v}^*) - j\omega c(\boldsymbol{u}^*, \boldsymbol{v}^*) - \omega^2 b(\boldsymbol{u}^*, \boldsymbol{v}^*) = l(\boldsymbol{P}, \boldsymbol{v}^*)\,, \ \ \forall \boldsymbol{v}^*$ in Ω (2′)

Eq. 2′ is a conjugate equation of the governing equation (Eq. 2) which governs $\boldsymbol{u}^*$, the conjugate complex of $\boldsymbol{u}$. It is important to note that the governing equation and its conjugate equation are used as constraints equations since the objective function contains the terms of $\boldsymbol{u}$ and $\boldsymbol{u}^*$.

3.3 Shape gradient function under a single frequency excitation

We derive the shape gradient function of the optimization problem using the adjoint variable method and the Lagrange multiplier method. The Lagrange functional L can be expressed as:

$$\begin{aligned} L =& \left|\int_\Omega \delta(\boldsymbol{x} - \boldsymbol{x}_0)\boldsymbol{u} \cdot \boldsymbol{u}^* \, d\Omega - \bar{u}_{x0}{}^2(\omega)\right| - \{a(\boldsymbol{u}, \boldsymbol{v}) + j\omega c(\boldsymbol{u}, \boldsymbol{v}) - \omega^2 b(\boldsymbol{u}, \boldsymbol{v}) - l(\boldsymbol{P}, \boldsymbol{v})\} \\ & -\{a(\boldsymbol{u}^*, \boldsymbol{v}^*) - j\omega c(\boldsymbol{u}^*, \boldsymbol{v}^*) - \omega^2 b(\boldsymbol{u}^*, \boldsymbol{v}^*) - l(\boldsymbol{P}, \boldsymbol{v}^*)\} + \Lambda(m - M) \end{aligned} \tag{9}$$

Here $\boldsymbol{v}$ and $\boldsymbol{v}^*$ are the adjoint variables, functioning as Lagrange multipliers. Additionally, Λ is introduced as the Lagrange multiplier associated with the mass constraint. The derivative of L with respect to variations in the domain, denoted as $\dot{L}$, can be obtained as follows:

$$\begin{aligned} \dot{L} = & -\{a(\boldsymbol{u}, \boldsymbol{v}') + j\omega c(\boldsymbol{u}, \boldsymbol{v}') - \omega^2 b(\boldsymbol{u}, \boldsymbol{v}') - l(\boldsymbol{P}, \boldsymbol{v}')\} \\ & -\{a(\boldsymbol{u}^*, \boldsymbol{v}^{*\prime}) - j\omega c(\boldsymbol{u}^*, \boldsymbol{v}^{*\prime}) - \omega^2 b(\boldsymbol{u}^*, \boldsymbol{v}^{*\prime}) - l(\boldsymbol{P}, \boldsymbol{v}^{*\prime})\} \\ & -\{a(\boldsymbol{u}', \boldsymbol{v}) + j\omega c(\boldsymbol{u}', \boldsymbol{v}) - \omega^2 b(\boldsymbol{u}', \boldsymbol{v})\} + \text{sign}(f\,(\omega)) \int_\Omega \delta(\boldsymbol{x} - \boldsymbol{x}_0)\boldsymbol{u}' \cdot \boldsymbol{u}^* \, d\Omega \\ & -\{a(\boldsymbol{u}^{*\prime}, \boldsymbol{v}^*) - j\omega c(\boldsymbol{u}^{*\prime}, \boldsymbol{v}^*) - \omega^2 b(\boldsymbol{u}^{*\prime}, \boldsymbol{v}^*)\} + \text{sign}(f\,(\omega)) \int_\Omega \delta(\boldsymbol{x} - \boldsymbol{x}_0)\boldsymbol{u} \cdot \boldsymbol{u}^{*\prime} \, d\Omega \\ & +\dot{\Lambda}(m - M) + l(\boldsymbol{G}, \boldsymbol{V}) \end{aligned} \tag{10}$$

where

$$l(\boldsymbol{G}, \boldsymbol{V}) = \int_\Gamma \ G n_i V_i d\Gamma \tag{11}$$

$$G(\boldsymbol{u}, \boldsymbol{v}) = -2\text{Re}\left[(1 + j\omega\beta) C_{ijkl} u_{k,l} v_{i,j} - (\omega^2 - j\omega\alpha)\rho u_i v_i\right] + \Lambda \tag{12}$$

In these equations, n_i is the components of the normal vector, $\text{Re}[\,\cdot\,]$ means the real part of a complex number, and G is called the shape gradient function. By satisfying Eqs. (13) to (15) below,

$$a(\boldsymbol{u}, \boldsymbol{v}') + j\omega c(\boldsymbol{u}, \boldsymbol{v}') - \omega^2 b(\boldsymbol{u}, \boldsymbol{v}') = l(\boldsymbol{P}, \boldsymbol{v}')\,, \ \ \forall \boldsymbol{v}' \text{ in } \Omega \tag{13}$$

$$a(\boldsymbol{u}', \boldsymbol{v}) + j\omega c(\boldsymbol{u}', \boldsymbol{v}) - \omega^2 b(\boldsymbol{u}', \boldsymbol{v}) = \text{sign}\big(f\,(\omega)\big) \int_\Omega \delta(\boldsymbol{x} - \boldsymbol{x}_0)\boldsymbol{u}' \cdot \boldsymbol{u}^* \, d\Omega, \ \forall \boldsymbol{u}' \text{ in } \Omega \tag{14}$$

$$m - M \leq 0\,, \dot{\Lambda}(m - M) = 0, \Lambda \geq 0 \tag{15}$$

we obtain the Eq. (16) as:

$$\dot{L} = l(\boldsymbol{G}, \boldsymbol{V}) = \int_{\Gamma} \; G n_i V_i d\Gamma \tag{16}$$

Equation (13) gives the governing equation for $\boldsymbol{u}$, equation (14) gives the adjoint equation for adjoint variable $\boldsymbol{v}$, and equation (15) defines the constraint equation on mass. Equation (16) implies that finding a velocity $\boldsymbol{V}$ such that $l(\boldsymbol{G}, \boldsymbol{V}) < 0$ ensures that the original objective function decreases towards a minimum.

3.4 Shape gradient function under a wideband frequency excitation

For the optimization problem of amplitude regulation with a wideband frequency excitation, the objective function is defined as the integral of the single-frequency objective function across the frequency domain. When the excitation frequencies vary from ω_1 to ω_2, the objective function can be written as:

$$F = \int_{\omega_1}^{\omega_2} \left| u_{x0}(\omega) \cdot {u_{x0}}^*(\omega) - {\bar{u}_{x0}}^2(\omega) \right| d\omega \tag{17}$$

In this case, the shape gradient function is given in Eq. (18).

$$G(\boldsymbol{u}, \boldsymbol{v}) = \int_{\omega_1}^{\omega_2} -2\,\mathrm{Re}[\,(1 + j\omega\beta) C_{ijkl} u_{k,l} v_{i,j} - (\omega^2 - j\omega\alpha)\rho u_i v_i] d\omega + \Lambda \tag{18}$$

3.5 Modal solution of the shape gradient function

To calculate the shape gradient function, both Eq. (2) and Eq. (14) must be solved for the frequency responses $\boldsymbol{u}$ and $\boldsymbol{v}$. There are primarily two methods to solve the frequency response: the direct method and the modal method. The latter has an advantage in computational efficiency when evaluating the frequency response over a wide frequency range. However, it requires the decoupling of the equation of motion, which cannot be conducted in this case due to the existence of dampers. In this study, we use a hybrid approach to solve both $\boldsymbol{u}$ and $\boldsymbol{v}$ with modal parameters as follows:

$$\boldsymbol{u} = \sum_{r=1}^{n} \xi_r \boldsymbol{u}_r \tag{19}$$

$$\boldsymbol{v} = \sum_{r=1}^{n} \eta_r \boldsymbol{u}_r \tag{20}$$

In the two equations, $\boldsymbol{u}_r$ denotes the *r*th eigenvector, while ξ_r and η_r represent the modal coordinates of $\boldsymbol{u}_r$, and *n* is the number of degrees of freedom. For each sampling frequency, ξ_r and η_r can be obtained by solving a system of simultaneous equations with *N* complex variables. Due to space limitations, the details of the calculations are omitted. Since the number of dampers *N* is typically much smaller than *n*, this approach can effectively reduce the computation time compared to directly solving the response with *n* degrees of freedom at each sampling frequency.

4. Construction of optimization system

We use the so-called the H^1 gradient method for shape optimization. The H^1 gradient method is a nonparametric technique for shape optimization [17]. This approach starts with an analytical derivation of the shape gradient function. It determines the optimal shape variation field by applying the shape sensitivity function as a pseudo-load on the design boundary to obtain the displacement field, which is then used to gradually refine the shape. By utilizing elastic deformation as the shape variation, this method has several advantages: it enables smooth shape changes without mesh refinement, eliminates the need for shape parameterization, and can be easily integrated with commercial finite element analysis (FEA) software.

The optimization system is established by combining general-purpose CAE software with a custom-developed program. The main procedures of the optimization system are shown in Fig. 6. During the modeling process, two models are created: one for modal analysis, and another for shape modification by H^1 gradient method. Each

optimization cycle includes one modal analysis, one calculation of shape gradient function, and one shape modification. From the modal analysis, the mode vectors and eigenvalues are obtained. The frequency response, adjoint variable, shape gradient function and objective function for each sampling frequency are calculate using the results from modal analysis. The optimization cycle is repeated until the objective function converges.

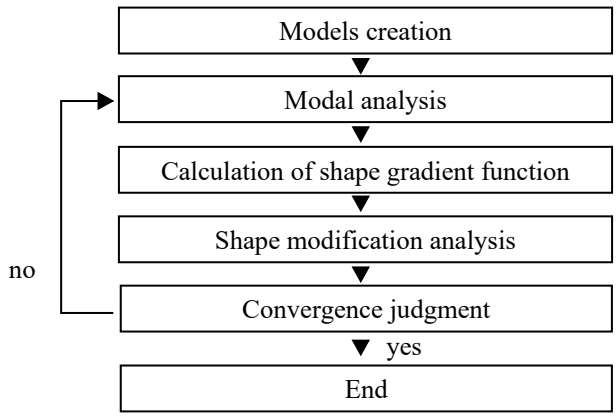

Fig. 6. Flow chart of optimization analysis system.

5. Numerical analyses and considerations

The optimization analysis of an idealized numerical model was conducted to confirm the validity of the proposed approach. Then, the shape optimization of a cartilage plate was performed, and the results were compared to those obtained using a flat plate.

5.1 Numerical example1: shape optimization of an idealized model

As a hypothetical model is employed, the material properties, dimensions, and frequencies are assigned non-dimensional values to simplify analysis. The FE model is shown in Fig. 7. The shape of the model is a plate-like 3D solid with uniform thickness of 1. The boundaries are fully constrained, and an excitation force is applied normal to the upper surface as pressure, with a frequency range from 0.01 to 1. A damper is placed at the center of the plate with a damping coefficient of $c_d = 0.4$. The material properties used are a young's modulus of $E = 2.8 \times 10^6$, a density of $\rho = 1.3 \times 10^3$, and a Poisson's ratio of $\mu = 0.3$. The coefficients of Rayleigh damping are set to $\alpha = 1.0$ and $\beta = 7.5 \times 10^{-5}$. The shape of the reference model is shown in Fig. 8. The objective of this analysis is to optimize the shape of plate so that the frequency response at the center point closely matches that of the reference model.

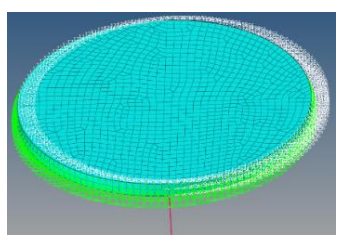

Fig. 7. FE model of a uniform plate with a damper.

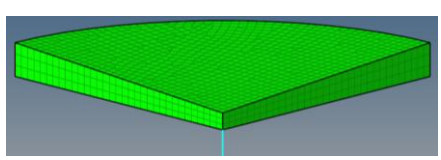

Fig. 8. Shape of the reference model.

5.2 Results and consideration of numerical example1

The optimized shape was obtained through this analysis, as shown in Fig. 9a (the overall view of the shape) and Fig. 9b (the cross-sectional view). From the cross-sectional view, it can be seen that the optimized shape resembles the reference model. Figure 10 illustrates the variation history of the objective function, which is the least squares difference between the amplitudes at the center points of the two models, and the mass ratio m/m_0. These results confirmed that the objective function decreased by 98%, while the mass remained approximately constant. This demonstrates that the proposed shape optimization approach worked effectively in this idealized model, confirming its validity before application to more realistic cases.

To further evaluate the effectiveness of the optimization, frequency response curves at the center point of the plate for both the optimized model and the reference model were compared, as shown in Fig. 11. In the target frequency range, the optimized design nearly coincides with the reference curve except in a narrow high-frequency region. This result indicates that the optimized shape successfully reproduces the desired vibration characteristics, and demonstrates the potential of the proposed method to design desired frequency response characteristics, which may find application in the mechanical engineering, such as vibration suppression and structural optimization.

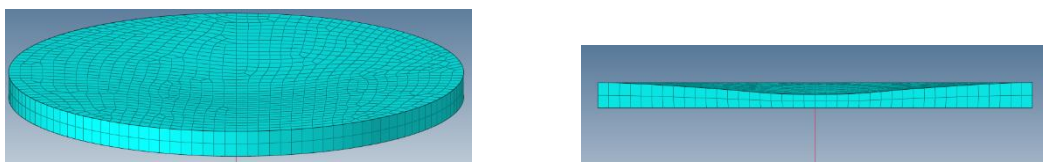

(a) Overall view of optimized shape (b) Cross section of the optimized shape

Fig. 9. Optimized shape with an excitation frequency range from 0.01~1.00.

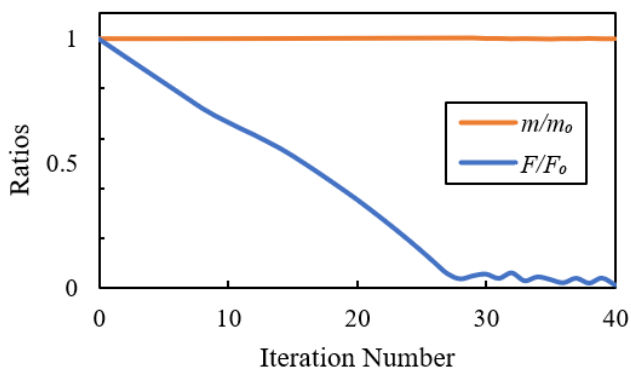

Fig. 10. Iteration histories of objective function and volume

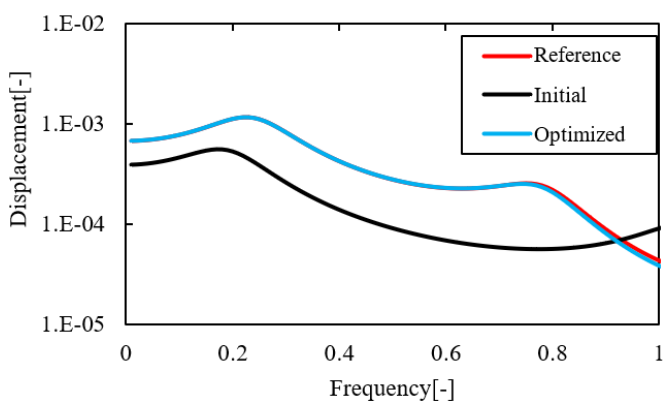

Fig. 11. Comparison of frequency response curves.

5.3 Numerical example2: shape optimization of a repaired TM model

The repaired TM model shown in Fig. 4(b) was used for the optimization. A flat plate with a thickness of 0.5 mm serves as the initial design. The thickness is constrained to a range of 0.1 mm to 0.9 mm. The target frequency range is set from 0.25 kHz to 2.0 kHz, which is the most important range for daily conversation.

5.4 Results and consideration of numerical example2

The thickness distribution of the cartilage plate after 45 iterations of optimization is shown in Fig. 12, with thickness expressed in color. It is observed that the thickness of the lower part of the TM approached the lower limit, while the upper part approached the upper limit. This analysis suggests that when repairing the TM with a cartilage plate, making the lower half of the membrane thinner is important for approximating conventional auditory characteristics. The upper half becomes thicker, likely because its thickness is less critical than in the lower half, and there is a constraint to maintain a constant volume of the TM. Figure 13 illustrates the iteration history of the objective function and the volume constraint. It is found that the objective function decreased monotonically as the analysis progressed, converging to 57% of the initial value, while the volume remained constant. This result indicates the effectiveness of the shape optimization. Figure 14 shows the frequency response of the stapes footplate after optimization. Compared to the initial design, it can be observed that within the target frequency range, the optimized design closely follows the reference curve in most areas. Additionally, the optimized design improves the problem of the reduction in peak position. Although shape optimization can improve auditory characteristics, a significant gap remains between the optimized curve and the reference curve. This discrepancy may be due to the large difference in material properties between the cartilage and the original TM, and further improvements rely on the development of new biomaterials. Fortunately, significant research has been conducted in this area. For example, Anand et al. investigated the tensile strength and acoustic properties of artificial TM materials, demonstrating that radial and circumferential pattern shapes play an important role in these functional properties [18].

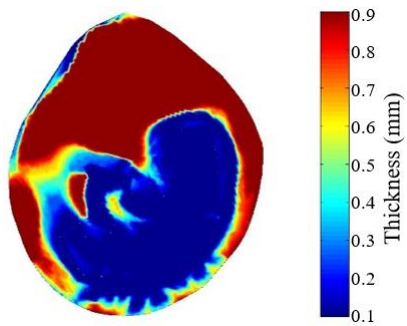

Fig. 12. Optimized thickness distribution of TM.

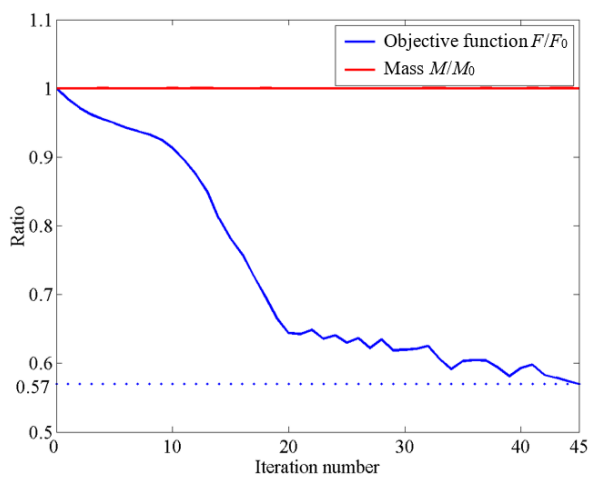

Fig. 13. Iteration history of the objective function and the volume constraint.

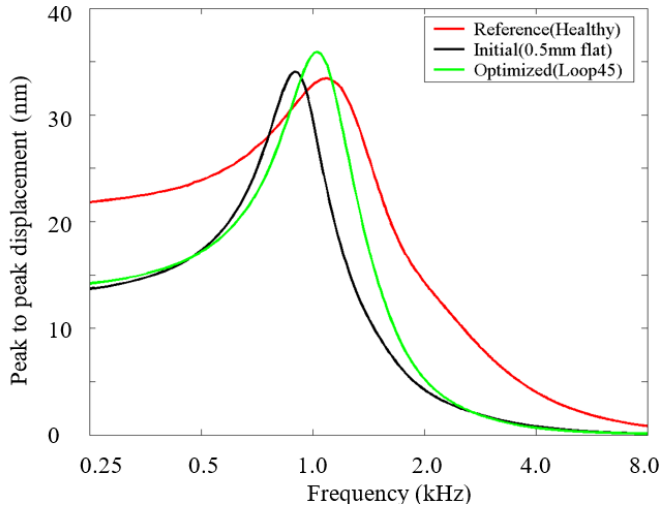

Fig. 14. Frequency response of the stapes footplate.

It should be noted that the optimal thickness distribution of the cartilage is likely to vary depending on the size and location of the tympanic membrane perforation. Therefore, this analysis only provides an optimal solution for the specific perforation area and location examined in this study. Moreover, this analysis result is considered solely from an engineering perspective. Some conditions for the analysis were set without significant consideration from a medical standpoint. For instance, the original geometric data was obtained from a 75-year-old male, and due to individual anatomical differences in middle ear structures, the medical representativeness of this data was not evaluated. Additionally, upper and lower limits were set for the cartilage plate thickness during the analysis, but whether these limits are medically appropriate has not been thoroughly considered. Furthermore, although the analysis results indicate an improvement in the middle ear's vibration characteristics, it remains uncertain whether this level of improvement holds clinical significance. Through this analysis example, we did not aim to obtain the optimal shape for TM repair, but rather to demonstrate that the proposed method shows potential utility in such types of analysis, paving the way for future applications in TM repair design.

6. Conclusion

In this paper, we presented an approach for shape optimization of a cartilage plate used in cartilage tympanoplasty to improve auditory characteristics after surgery. A finite element model was developed and validated by comparing the analysis results with measured data. Using this model, we confirmed the differences in auditory characteristics when repairing TM perforations with a cartilage plate compared to the original healthy state. We formulated a shape optimization approach to minimize the least squares difference between the amplitudes of the stapes post-repair and those in the healthy state across a wide frequency range. To enhance computational efficiency, the shape gradient function was derived and calculated using modal parameters. The H^1 gradient method was employed for shape modification. Numerical examples were conducted to demonstrate the effectiveness of our approach. The analysis results indicated that shape optimization of the cartilage plate can lead to a certain level of improvement in auditory characteristics. However, to achieve further enhancement, the development of advanced biomaterials that more closely match the properties of the native TM may also be necessary. Additionally, as this study was conducted primarily from an engineering perspective, to determine the real-world applicability of this approach, further medical evaluation is necessary to confirm its clinical relevance and address individual anatomical differences in middle ear structures.

Acknowledgments

This work was supported by JSPS KAKENHI Grant Number JP21k03820.

References

[1] Wada H, Kobayashi T, Metoki T. Modeling of the human middle ear using the finite-element method. Transactions of the Japan Society of Mechanical Engineers, Series C. 1990;56(532):3191–3195.

[2] Wada H, Kobayashi T, Hashimoto S, Kobayashi N. Modeling of human middle ear using finite-element method (2nd report, introduction of the functions of muscles, ligaments and joint of ossicles). Transactions of the Japan Society of Mechanical Engineers, Series C. 1992;58(554):3050–3055.

[3] Gan RZ, Sun Q, Dyer RK, Chang KH, Dormer KJ. Three dimensional modeling of middle ear biomechanics and its applications. Otology & Neurotology. 2002;23(3):271–280.

[4] Koike T, Wada H. Modeling of the human middle ear using the finite-element method. The Journal of the Acoustical Society of America. 2002;111(3):1306–1317.

[5] Wada H, Koike T, Matsutani S, Kobayashi T, Takasaka T. Dynamic behavior of middle ear with tympanic membrane perforation – Theoretical analysis using finite-element method. Audiology Japan. 1997;40:46–51.

[6] Gan RZ, Cheng T, Dai CK, Yang F, Wood WM. Finite element modeling of sound transmission with perforations of tympanic membrane. The Journal of the Acoustical Society of America. 2009;126(1):243–253.

[7] Greef DD, Buytaert JA, Aerts JRM, Van Hoorebeke L, Dierick M, Dirckx J. Details of human middle ear morphology based on micro-CT imaging of PTA stained samples. Journal of Morphology. 2015;276(9):1025–1046.

[8] Zahnert T, Huttenbrink KB, Mürbe D, Bornitz M. Experimental investigation of the use of cartilage in tympanic membrane reconstruction. American Journal of Otolaryngology. 2000;21(3):322–328.

[9] Lee CF, Chen JH, Chou YF, Hsu LP, Chen PR, Liu TC. Optimal graft thickness for different sizes of tympanic membrane perforation in cartilage myringoplasty: A finite element analysis. Laryngoscope. 2007;117(4):725–730.

[10] Torisaki M, Shimoda M, Ali MA. Shape optimization method for strength design problem of microstructures in a multiscale structure. International Journal for Numerical Methods in Engineering. 2023;124(8):1748–1772.

[11] Gröhlich M, Böswald M, Wallaschek J. Viscoelastic damping design – A novel approach for shape optimization of constrained layer damping treatments at different ambient temperatures. Journal of Sound and Vibration. 2023;555:117703.

[12] Greef DD, Buytaert JA, Aerts JRM, Van Hoorebeke L, Dierick M, Dirckx J. Laboratory of Biomedical Physics, University of Antwerp [Internet]. [cited 2020 Sep 2]. Available from: https://www.uantwerpen.be/en/research-groups/bimef/downloads/middle----inner--ear/human--homo-sapiens-/

[13] Garcia-Gonzalez A, Castro-Egler C, Gonzalez-Herrera A. Analysis of the mechano-acoustic influence of the tympanic cavity in the auditory system. BioMedical Engineering OnLine. 2016;15(33):1–20.

[14] Greef DD, Pires F, Dirckx JJJ. Effects of model definitions and parameter values in finite element modeling of human middle ear mechanics. Hearing Research. 2017;344:195–206.

[15] Dai C, Cheng T, Wood MW, Gan RZ. Fixation and detachment of superior and anterior malleolar ligaments in human middle ear: Experiment and modeling. Hearing Research. 2007;230(1–2):24–33.

[16] Sokolowski J, Zolésio JP. Introduction to Shape Optimization: Shape Sensitivity Analysis. New York: Springer-Verlag; 1991.

[17] Azegami H. Solution to domain optimization problems. Transactions of the Japan Society of Mechanical Engineers, Series A. 1994;60(574):1479–1486.

[18] Anand S, Stoppe T, Lucena M, Rademakers T, Neudert M, Danti S, Moroni L, Mota C. Mimicking the human tympanic membrane: The significance of scaffold geometry. Advanced Healthcare Materials. 2021;10(11):e2100077.